

# SUPPLEMENTARY INFORMATION

## Heterojunctions of Halogen-Doped Carbon Nitride Nanosheets and BiOI for Sunlight-Driven Water-Splitting

Kazi M. Alam,<sup>1†</sup> Pawan Kumar,<sup>1†</sup> Piyush Kar,<sup>1</sup> Ankur Goswami,<sup>1</sup> Ujwal K. Thakur,<sup>1</sup> Sheng Zeng,<sup>1</sup> Ehsan Vahidzadeh,<sup>1</sup> Kai Cui<sup>2</sup> and Karthik Shankar<sup>1\*</sup>

<sup>1</sup>*Department of Electrical & Computer Engineering, University of Alberta, Edmonton, AB T6G 1H9 Canada*

<sup>2</sup>*Nanotechnology Research Centre, National Research Council of Canada, Edmonton, Canada*

\*corresponding author's email address: [kshankar@ualberta.ca](mailto:kshankar@ualberta.ca)

†These authors contributed equally

### 1. Experimental Section

#### 1.1 Synthesis of pristine CNF-Cl, pristine BiOI and BiOI/CNF-Cl composite

The synthesis of fluorine-doped and chlorine-intercalated carbon nitride sheets (CNF-Cl) was realized by the previously reported protocols by high temperature annealing of dicyandiamide, NH<sub>4</sub>F and NH<sub>4</sub>Cl precursors. [1-3] In this synthesis dicyandiamide works as a source of carbon and nitrogen and forms tertiary N-linked tris-s-triazine (heptazine; C<sub>6</sub>N<sub>7</sub>) polymeric framework (g-C<sub>3</sub>N<sub>4</sub>) *via* condensation polymerization. Continuous repetition of heptazine units creates conjugated semiconductor network of carbon nitride. Ammonium fluoride facilitate F-doping in heptazine motifs and F atoms get bounds to bay and corner carbon atoms which partially destroy

---

\* Tel: 780-492-1354; email: kshankar@ualberta.ca

the symmetry of conjugated network resulting into band gap reduction due to shifting of HOMO and LUMO positions.[1] While excess of  $\text{NH}_4\text{Cl}$  facilitate *in-situ* sheets formation due to release of  $\text{NH}_3$  and  $\text{HCl}$  gases at elevated temperature that blew dicyandiamide-derived polymers into numerous large bubbles, affording fluorine doped carbon nitride nanosheets.[2] In addition, the use of excess  $\text{NH}_4\text{Cl}$  also render chlorine intercalation between F-doped g- $\text{C}_3\text{N}_4$  layers which provides interlayer galleries for better charge migration. Furthermore, intercalated chlorine also reduces the band gap and uplifting of conduction band (advantageous for proton reductions).[1-3] In brief, 2 g dicyandiamide, 0.5 g  $\text{NH}_4\text{F}$  and 10 g  $\text{NH}_4\text{Cl}$  were mixed together by grinding in a mortar. The obtained powder mixture was dispersed in 100 mL water followed by heating at 100 °C until all the water evaporated. The obtained dry solid was crushed and heated in a tube furnace using a programmed heating rate of 5 °C  $\text{min}^{-1}$  up to 400 °C; 2 °C  $\text{min}^{-1}$  up to 500 °C, and 1 °C  $\text{min}^{-1}$  up to 550 °C followed by holding at 550 °C for 2 h. After completion of the heating step, the afforded solid was allowed to cool down to room temperature. Finally, the obtained yellow CNF-Cl solid was finely ground in a mortar and stored to be used for subsequent steps.

The BiOI/CNF-Cl heterostructure synthesis was achieved by an *in-situ* hydrothermal protocol available in the literature[4-6] with minor modifications. Bismuth nitrate pentahydrate,  $\text{Bi}(\text{NO}_3)_3 \cdot 5\text{H}_2\text{O}$  and KI were used as Bi and I precursors respectively. To synthesize BiOI and CNF-Cl composites, certain amount of  $\text{Bi}(\text{NO}_3)_3 \cdot 5\text{H}_2\text{O}$  and CNF-Cl (340 mg) were dispersed in 20 mL ethylene glycol (EG) and ultrasonicated until a homogeneous solution was achieved. Separately, a stoichiometric amount of KI was dissolved in ethanol and ultrasonicated to obtain a transparent solution. In the next step, we added the KI solution drop-by-drop into the solution containing  $\text{Bi}(\text{NO}_3)_3 \cdot 5\text{H}_2\text{O}$  and CNF-Cl under vigorous stirring. After continuously stirring this final solution for an additional 30 min, the obtained solution was transferred into a Teflon-lined

stainless-steel autoclave and heated at (150 °C) for 15 h. Pristine BiOI was synthesized using  $\text{Bi}(\text{NO}_3)_3 \cdot 5\text{H}_2\text{O}$  and KI alone without adding CNF-Cl by following the same steps of composite formation. After natural cooling, the pristine BiOI and BiOI/CNF-Cl composite solutions were washed several times with methanol and DI water using centrifugation to eliminate any unreacted species. Finally, the solid precipitates were collected and dried in an oven at 60 °C overnight. We have studied composites with variable weight percentage (10, 25, 50 and 75%) of BiOI in this work. The highest photoelectrochemical performance was observed for 50 wt% BiOI with CNF-Cl. In the rest of this article, we have denoted these samples as BiOI/CNF-Cl.

## ***1.2 Characterization***

*Transmission Electron Microscopy (TEM).* The imaging and elemental analyses (EDX) of BiOI/CNF-Cl composite and pristine CNF-Cl samples were conducted using a JEOL 2200 FS transmission electron microscope equipped with a field emission gun with an accelerating voltage of 200 kV. EDX mapping was performed under scanning TEM (STEM) mode with a nominal probe size of 1 nm. Prior to the analysis, BiOI/CNF-Cl composite and pristine CNF-Cl powders were dispersed in ultra-dilute suspensions in methanol, sonicated for 30 min and then deposited on lacey carbon-coated copper TEM grids. The TEM grids were kept underneath a solar simulator under AM1.5G one sun illumination for one h to evaporate any residual solvent before TEM analysis.

*Field Emission Scanning Electron Microscopy (FESEM).* The morphology of the composite film (50% BiOI/CNF-Cl) was studied using a Zeiss Sigma FESEM with an accelerating voltage of 5 kV.

*X-Ray Diffractometry (XRD).* The pristine and composite catalysts were characterized by powder XRD on a Bruker D8 advance X-ray diffractometer with a  $\text{Cu K}\alpha$  radiation source ( $\lambda = 1.5406$

Å) operating at 50 W at room temperature and equipped with a 2-D detector (VANTEC-500).

*Fourier Transfer Infrared Spectroscopy.* Fourier transform infrared (FTIR) spectra were measured using an Agilent FTS7000 FTIR Imaging System equipped with diamond ATR (attenuated total reflection). FTIR data were recorded in transmittance mode in the 400–4000  $\text{cm}^{-1}$  frequency range. Powder samples were placed on the clean diamond crystal, prior to the collection of the spectra, while moderate nitrogen gas flow was maintained through the ATR assembly.

*Raman Spectroscopy.* A Nd:YAG laser Raman Microscope (Nicolet Omega XR) was used to collect the Raman spectra of the pristine and composite photocatalysts. The excitation wavelength of the laser was 785 nm with a power of 7 mW. The fluorescence correction factor was set to as high as 4. The other experimentally relevant parameters were an aperture size of 50  $\mu\text{m}$  and 900 lines/mm grating.

*Absorption Spectroscopy.* The optical properties of the pristine and composite materials were obtained using diffuse reflectance UV–Vis-NIR spectrometry (DRS). A Perkin Elmer Lambda 1050 UV-Vis-NIR spectrophotometer equipped with an integrating sphere accessory was used to collect the absorption spectra over the range 250-800 nm.

*Steady State Photoluminescence (SSPL) and Time Resolved Photoluminescence (TRPL) Spectroscopy.* Steady state photoluminescence (SSPL) spectra were collected using a Varian Cary Eclipse fluorimeter using an excitation wavelength of 360 nm. A homemade single photon counting system with a response time of  $\sim 100$  ps, was used to collect the time resolved photoluminescence (TRPL) spectra. A 405-nm picosecond diode laser (Alphas GmbH) operating at a frequency of 1 MHz, was used to photoexcite the samples. The emission was detected by a Becker-Hickl HPM-100-50 PMT interfaced to an SPC-130 pulse counter system.

*Kelvin Probe Force Microscopy (KPFM)*. A Dimension fast scan atomic force microscope (Bruker Nanoscience Division, Santa Barbara, CA, USA) was used to measure the change in surface potential (SP) or contact potential difference (CPD) of pristine BiOI, pristine CNF-Cl and composite (50 % BiOI/CNF-Cl) photocatalysts. The measurements were performed in the presence and absence of a 450 nm wavelength diode laser which illuminated the samples at normal incidence. A SCM-PIT cantilever was used in this experiment. The cantilever has 4.4 N/m stiffness. The surface potentials of the samples were measured at 75 nm lift height at 2 kHz lock-in bandwidth by maintaining a scan speed of 1 Hz. Prior to the experiment, conducting copper tape was used to ground the samples with the AFM chuck. The surface potential was mapped by sample routing at zero tip bias. Prior to the experiments, dark and illumination conditions were maintained for 5 min, in order to achieve steady state. The work function of the Pt-Ir tip was calibrated by measuring the contact potential difference (CPD) of HOPG and the Pt tip using the following equation:  $EF(\text{tip}) = 4.6 \text{ eV (Work function of HOPG)} + V_{\text{CPD}}(\text{HOPG and Pt tip})$ . The value of the work function was found to be 5.04 eV.

### ***1.3 Photoelectrochemical testing***

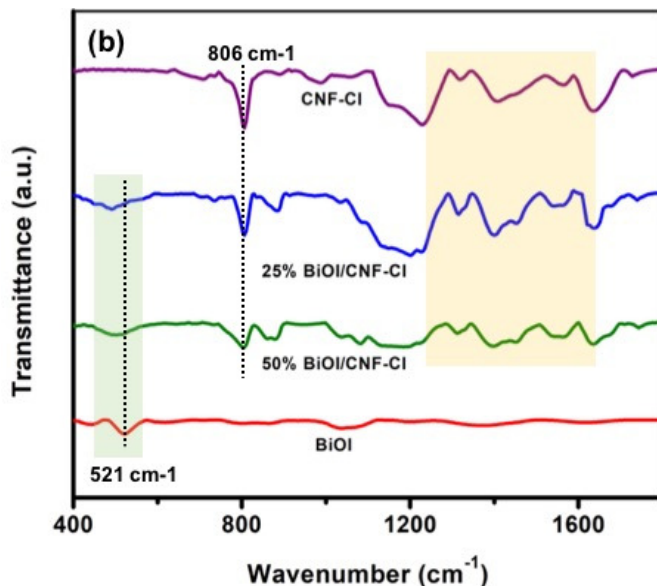
A three-electrode set-up (CHI 600D potentiostat) was used for photoelectrochemical water splitting experiments. Pristine BiOI, pristine CNF-Cl and BiOI/CNF-Cl composite films were prepared on fluorine doped tin oxide (FTO) coated glass. An ultra-thin (~ 50 nm) compact layer of  $\text{TiO}_2$ [7] was deposited on cleaned (water, ethanol and acetone sonicated) FTO prior to the drop coating of the catalyst powders. Catalyst materials were dissolved in alpha-terpineol ( $30 \text{ mg mL}^{-1}$ ) and stirred for 60 min before dropping on the FTO. Alpha-terpineol was used as a binder and evaporated later on a hot plate at  $200 \text{ }^\circ\text{C}$ . This as-prepared sample on FTO was used as the working electrode (photoanode) and Pt was used as the counter electrode (cathode). An Ag/AgCl glass

electrode was used as the reference electrode. The electrodes were immersed in an aqueous 0.1 M Na<sub>2</sub>SO<sub>4</sub> electrolyte solution. The photocurrent response of the photocatalysts was monitored by linear sweep voltammetry from -0.8 V to +0.8 V with a scan rate of 10 mV/sec. The samples were irradiated with AM1.5G one sun simulated sunlight from a class A solar simulator (Newport-Oriel Instruments USA). The illumination intensity measured at the surface of photoanode was 100 mW cm<sup>-2</sup>. In order to probe the visible light induced photocurrent response, the samples were also illuminated in separate experiments using LEDs (425 and 505 nm) with an incident power density of 47.70 mW cm<sup>-2</sup> and 40.48 mW cm<sup>-2</sup> respectively at the surface of the photoanode. To determine the hydrogen evolution rate and Faradaic efficiency, photoelectrochemical water splitting was performed in an H cell, under AM1.5 G irradiation and evolved hydrogen was collected on Pt counter electrode (Figure S6). The gaseous sample from the Pt counter electrode arm was withdrawn after 2 h interval using a gas-tight syringe and analyzed using gas chromatography, specifications: custom made Shimadzu GC equipped with Porapak Q and Mol Sieve column and pulsed discharge detector (PDD). Conditions: carrier gas (Helium), flow rate: 0.5 mL min<sup>-1</sup>, detector temperature: 160 °C, oven temp: started from 60 °C and ramped up to 160 °C. For the identification and quantifying the reaction product, a calibration gas mixture (Praxair gas, Canada) was used as a standard.

Electrochemical impedance spectroscopy (EIS) was performed using a regular one-compartment electrochemical cell with a three-electrode configuration at an applied voltage of -0.5 V vs Ag/AgCl in 0.1 M Na<sub>2</sub>SO<sub>4</sub>. Impedance spectra were recorded at 1 kHz, and the amplitude of the superimposed sinusoidal potential signal was 5 mV. Mott-Schottky plots were collected from impedance-potential measurements at 1 kHz frequency in the voltage range from -1.0 to +1.0 V.

## 2.0 Fourier transform infrared spectroscopy (FTIR):

Fourier transform infrared spectroscopy (FTIR) was performed in order to further analyze the structural and vibrational features of the nanocomposites. Carbon nitride heterocycle (C-N)



stretching modes were assigned to the peaks between  $1240$  to  $1640 \text{ cm}^{-1}$  (light orange shaded region, Figure S1).[8] The characteristic breathing mode observed at  $806 \text{ cm}^{-1}$ , which originates due to bending vibration of *s*-triazine units, was found to be slightly shifted to higher wavenumbers from the typically observed peak location of  $802 \text{ cm}^{-1}$  for  $g\text{-C}_3\text{N}_4$ . [9, 10] The addition of fluorine in the carbon nitride network through doping can lead to this slight shifting. The peak around  $521 \text{ cm}^{-1}$ , associated with Bi-O stretching vibrations in BiOI, appears in both pristine BiOI and the composites, indicative of the presence of BiOI in the CNF-Cl scaffold.[11] However, contrary to the previously reported work[6], we observed a small shift of this peak towards a slightly lower wavenumber, possibly implying the strong interaction between BiOI and CNF-Cl, prepared by *in situ* hydrothermal route.

**Figure S1.** FTIR transmittance plots of pristine CNF-Cl, BiOI/CNF-Cl composites and pristine BiOI.

### 3.0 Calculation of efficiencies:

#### 3.1 Applied bias photon-to-current efficiency percentage (ABPE%):

Further, diagnostic efficiencies were calculated to explore performance of materials under applied bias and irradiation conditions.[12, 13] The applied bias photon-to-current efficiency percentage (ABPE%) which is a measure of photo-conversion efficiency (PCE) under applied potential was determined by plotting a graph between ABPE% and applied voltage on RHE (reversible hydrogen electrode) scale. The ABPE% can be calculated by using following expression:

$$ABPE (\%) = [J (mA cm^{-2}) \cdot \frac{1.23-V_b}{P(mW cm^{-2})}] \cdot 100 \quad (1)$$

Where,  $J$  is the current density,  $V_b$  is applied voltage at RHE scale and  $P$  is power density of the incident light. The applied voltage on Ag/AgCl scale was converted to RHE scale using following expression:

$$V_{RHE} = V_{Ag/AgCl} + 0.059 \text{ pH} + V^0_{Ag/AgCl} \quad (2)$$

where  $V^0_{Ag/AgCl} = 0.197$  V. The applied bias photon-to-current efficiency (ABPE%) of pristine CNF-Cl and BiOI were found to be 0.08 and 0.11 % respectively while ABPE% of 10% BiOI/CNF-Cl, 25% BiOI/CNF-Cl, 50% BiOI/CNF-Cl and 75% BiOI/CNF-Cl heterostructures were calculated to be 0.09, 0.31, 0.71, and 0.34 % respectively.

#### 3.2 Incident Photon to Current Efficiency (IPCE%)

IPCE% also referred as external quantum efficiency (EQE) of the photoanodes was calculated under 425 nm and 505 nm irradiation and applied voltage of +0.6 V vs Ag/AgCl (1.23 V vs RHE, thermodynamic water splitting potential) using the following expression:

$$IPCE (\%) = \left[ \frac{1240 \cdot J (mA cm^{-2})}{\lambda (nm) \cdot P (mW cm^{-2})} \right] 100 \quad (3)$$

Where,  $J$  is photocurrent density,  $\lambda$  is wavelength of incident light in nm and  $P$  is the power density of incident light. The IPCE% of CNF-Cl, BiOI and 50% BiOI/CNF-Cl were calculated to be 0.43, 0.64 and 1.29% at 425 nm and 0.24, 0.36 and 1.09 % at 505 nm irradiation.

### 3.3 Absorbed Photon to Current Efficiency (APCE%)

A certain fraction of light remains unabsorbed and does not participate in electron hole pair generation. Therefore, APCE also referred as internal quantum efficiency (IQE) which measure photocurrent collected per incident photon absorbed is a good parameter to express the performance of materials while taking account of photon loss. The APCE% can be calculated by following expression:

$$APCE (\%) = (IPCE/absorptance) \times 100 \quad (4)$$

where the absorptance or light harvesting efficiency (LHE) demonstrates the number of electron hole pairs produced per incident photon flux. Assuming each absorbed photon produce equivalent electron hole pairs the value of absorptance can be calculated by Beer's law using the following equation:

$$APCE (\%) = \left[ \frac{1240 \cdot J (mA cm^{-2})}{\lambda (nm) \cdot P (mW cm^{-2}) \cdot (1 - 10^{-A})} \right] \cdot 100 \quad (5)$$

Where,  $J$  is photocurrent density,  $\lambda$  is wavelength of incident light in nm,  $P$  is the power density of incident light,  $LHE$  is light harvesting efficiency and  $A$  is absorbance at measured wavelength. The APCE% for CNF-Cl, BiOI and BiOI/CNF-Cl under 425 nm irradiation was calculated to be 0.53, 0.73 and 1.61 while under 505 nm these values was found 0.49, 0.42 and 1.54 % respectively.

### 3.4 Faradaic efficiency (FE%)

Faradaic efficiency is a measure of the actual fraction of photogenerated charge carriers participating in PEC water splitting reaction and can be defined as the ratio of observed  $H_2$  under experimental condition divided by theoretically evolved  $H_2$  calculated from photocurrent density.

$$\text{Faradaic efficiency (\%)} = \left[ \frac{\text{Experimental gas evolution (measured H}_2\text{)}}{\text{Theoretical H}_2\text{ gas evolution (based on photocurrent)}} \right] \cdot 100 \quad (6)$$

$$\text{Faradaic efficiency (\%)} = \left[ \frac{\text{H}_2\text{ evolution measured (mol)}}{\frac{J (\text{A cm}^{-2}) \cdot A (\text{cm}^2) \cdot T (\text{sec})}{2 \cdot e (\text{C}) \cdot N_A (\text{mol}^{-1})}} \right] \cdot 100 \quad (7)$$

Where,  $J$  is the photocurrent density ( $\text{A cm}^{-2}$ ),  $A$  is the irradiated area of electrode ( $\text{cm}^2$ ),  $T$  is the time of PEC measurement (seconds),  $e$  is the electronic charge ( $1.602 \times 10^{-19}$  C) and  $N_A$  is the Avogadro constant ( $6.02 \times 10^{23} \text{ mol}^{-1}$ ), the amount of hydrogen generated during PEC is expressed in moles.

#### **4.0 Electrochemical impedance spectroscopy (EIS)**

The pristine materials and nanocomposites were analyzed for their semiconductor electrolyte interfacial (SEI) behavior using electrochemical impedance spectroscopy (EIS). Representative EIS Nyquist plots are shown in Figure S2a and were obtained under dark and AM1.5 G one sun illumination in the frequency range of 0.1 to 100,000 Hz, at an applied bias of -0.4 V vs Ag/AgCl. Experimentally obtained EIS Nyquist plots were fitted using the equivalent circuit shown in the inset of Figure S2a and S3. Therein,  $R_s$ ,  $R_C$ ,  $R_T$ ,  $C_{SC}$ , and  $C_H$  are electrolyte resistance, charge transfer resistance, charge transport resistance, space charge capacitance, and electrochemical double-layer capacitance, respectively.  $Q$  is a constant phase element with coefficient  $n$ . The fitted values of circuit parameters are listed in Table S1 and fitted Nyquist plots are shown in Figure S2a. Recombination lifetime ( $\tau$ ) in the bulk was calculated using eq. 8 and is listed in Table S1, for all the samples. Long-lived holes are implied for the 25% BiOI/CNF-Cl from its higher recombination lifetime of 2.4  $\mu\text{s}$ . Shortened recombination lifetime with increased BiOI content, *i.e.* for 50% BiOI/CNF-Cl, is also evident. Low charge transfer resistances (of 1 Ohm) are obtained for CNF/Cl and the heterojunction samples (25% and 50% BiOI/CNF-Cl) from the Nyquist plots, and are indicative of lower resistance to hole transfer at the electrolyte interface.

$$\tau = R_T C_{SC} \quad (8)$$

$$\frac{1}{C_{SC}^2} = \frac{2}{e \epsilon_0 \epsilon_r N_D} \left\{ (V - V_{FB}) - \frac{kT}{e} \right\} \quad (9)$$

$$N_D = \frac{2}{e \epsilon_0 \epsilon_r} \left\{ \frac{dV}{dC_{SC}^2} \right\} \quad (10)$$

The Mott-Schottky equation (eq. 9) was used to calculate the charge carrier concentration ( $N_D$ ), and flat band potential ( $V_{FB}$ ). In eqs. 9 and 10,  $C_{SC}$  is space-charge capacitance per unit area;  $\epsilon_r$  the dielectric constant of the samples, which may be assumed to be 62 for CNF-Cl (i.e. same as dielectric constant for g-C<sub>3</sub>N<sub>4</sub>[14], and 73 for BiOI [15]). Dielectric constant of 25% BiOI/CNF-Cl was assumed to be same as CNF-Cl and that for 50% BiOI/CNF-Cl to be same as BiOI. Also, in eqs. 9 and 10,  $\epsilon_0$  is the vacuum permittivity ( $8.854 \times 10^{-14}$  F cm<sup>-1</sup>);  $k$  is Boltzmann constant ( $1.381 \times 10^{-23}$  J K<sup>-1</sup>);  $T$  is temperature in (298 K);  $e$  is the electron charge ( $1.602 \times 10^{-19}$  C); and  $V$  is the applied potential.  $V_{FB}$ , the flat band potential, is obtained from the point of intersection of the slope of the Mott-Schottky plot (Figure S2b) with the potential axis, as shown in Figure S4. The calculated  $V_{FB}$  values for CNF-Cl, BiOI, 25% BiOI/CNF-Cl, and 50% BiOI/CNF-Cl were found to be -0.66, -0.617, -0.720, -0.874 eV vs Ag/AgCl as displayed in Figure S4. Since band positions in photocatalysis are usually expressed in the NHE scale,  $V_{FB}$  of CNF-Cl, BiOI, 25% BiOI/CNF-Cl, and 50% BiOI/CNF-Cl were calculated to be -0.461, -0.418, -0.521 and -0.675 vs NHE scale at pH 0. The Mott-Schottky plots (Figure S2b and Figure S4) reveal that both the pristine semiconductor samples and the heterojunctions are *n*-type as the  $C^{-2}$ - $V$  curves have positive slopes. Figure S4 shows that the charge carrier density at equilibrium for 50% BiOI/CNF-Cl is 8 and 30 times higher than that of pristine CNF-Cl and pristine BiOI respectively.

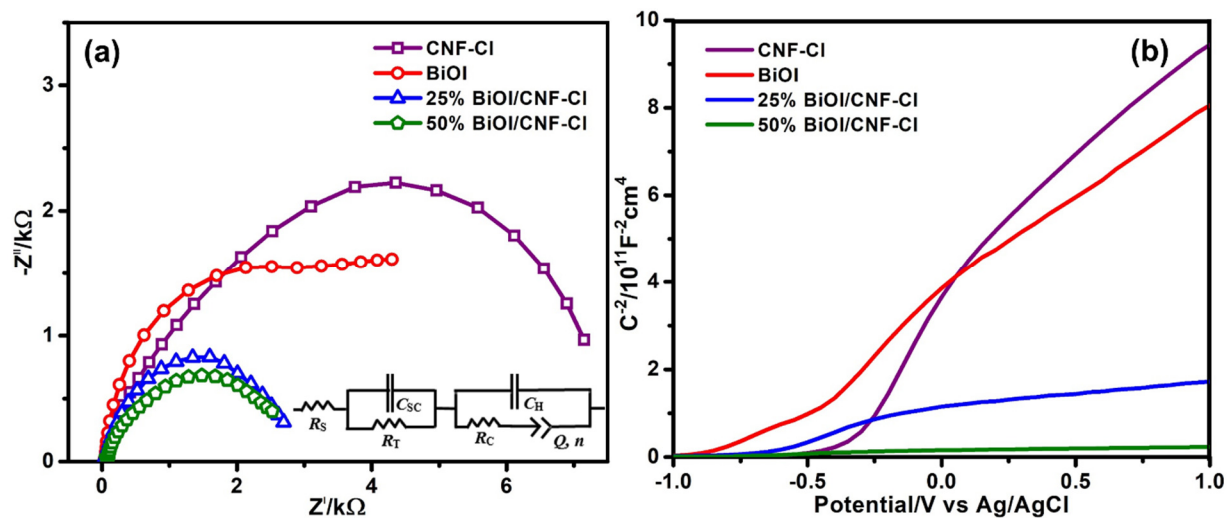


**Figure S2.** (a) Nyquist plots and (b) Mott-Schottky plots for pristine CNF-Cl, pristine BiOI and BiOI/ CNF-Cl composite photocatalysts obtained from electrochemical impedance spectroscopy (EIS). Inset of (a) Equivalent circuit used to model the EIS Nyquist plots for the pristine and composite photocatalysts. Data were collected using AM1.5 G one sun illumination while the frequency range was set from 0.1 to 10000 Hz at a potential of -0.2 V vs Ag/AgCl.

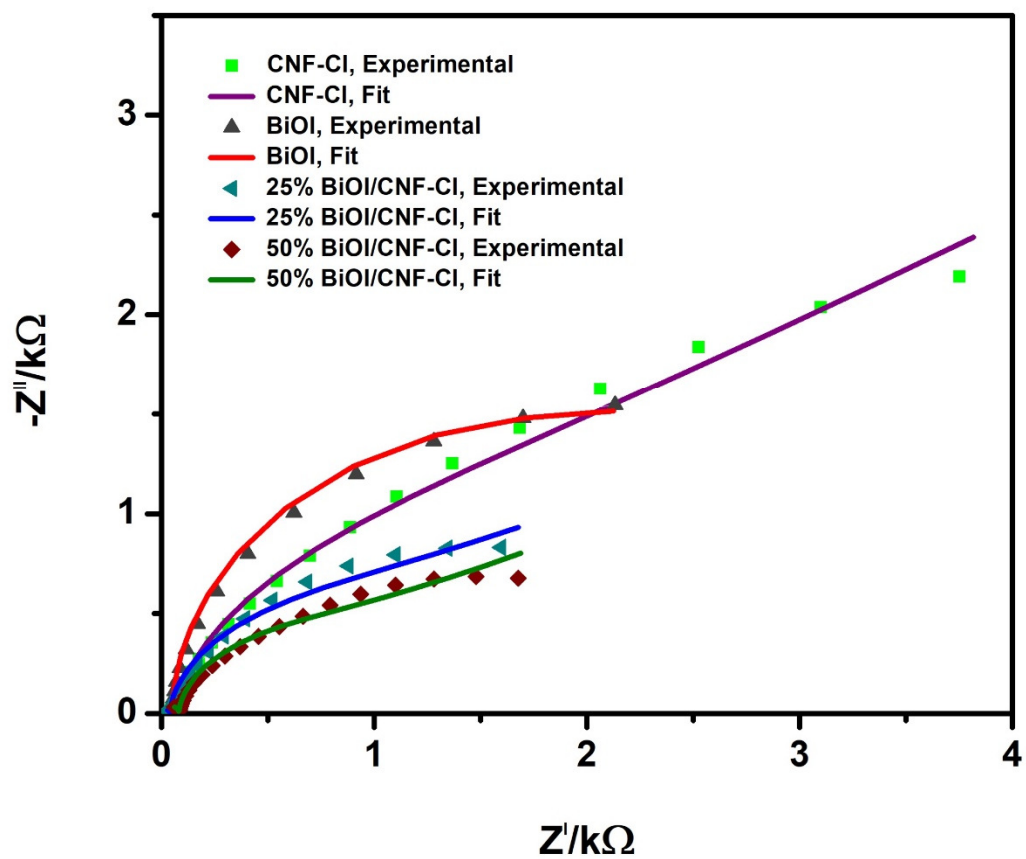


**Figure S3.** Fitted EIS Nyquist plots for obtaining the equivalent circuit (Fig. 7a. inset in main manuscript).

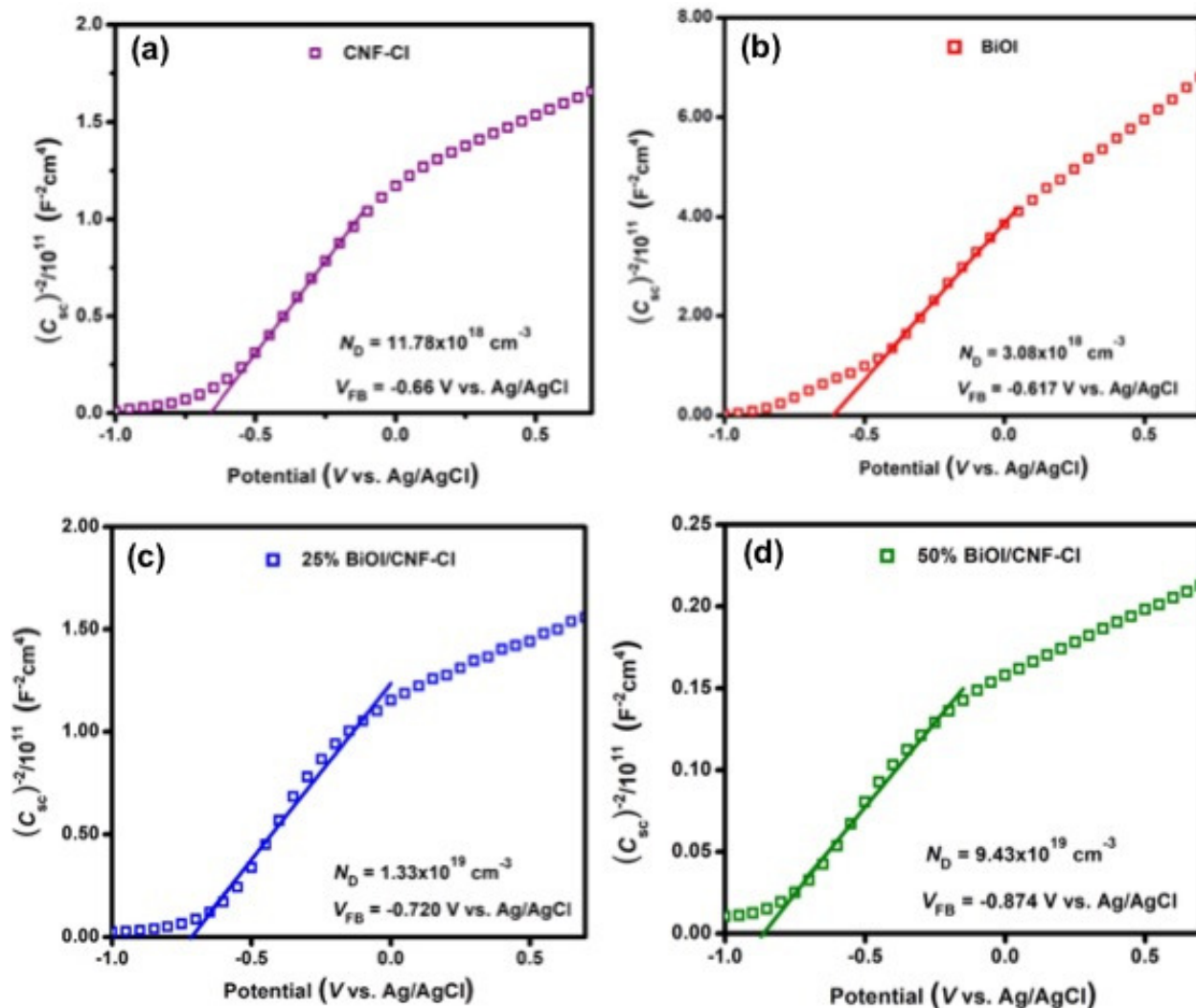


**Figure S4.** Mott-Schottky plots of (a) pristine CNF-Cl, (b) pristine BiOI, (c) 25% BiOI/CNF-Cl, and (d) 50% BiOI/CNF-Cl.

**Table S1.** Obtained electrochemical parameters by fitting Nyquist plots to the circuit shown in the inset of Figure S2a.

Sample	$R_s$ (Ohms)	$C_{sc}$ (F)	$R_T$ (Ohms)	$C_H$ (F)	$R_c$ (Ohms)	$Q$ ( $Fs^{-(1+n)}$ )	$n$	$\tau$ ( $\mu s$ )
CNF-Cl	10	$3.00 \times 10^{-8}$	60	$1.40 \times 10^{-6}$	1	$1.05 \times 10^{-4}$	0.33	1.80

<b>BiOI</b>	10	$4.50 \times 10^{-8}$	40	$1.60 \times 10^{-5}$	1450	$3.00 \times 10^{-4}$	0.30	1.80
<b>25% BiOI/CNF-CI</b>	10	$8.00 \times 10^{-8}$	30	$5 \times 10^{-6}$	1	$2.75 \times 10^{-4}$	0.28	2.40
<b>50% BiOI/CNF-CI</b>	10	$2.20 \times 10^{-8}$	70	$3.50 \times 10^{-6}$	1	$3.30 \times 10^{-4}$	0.23	1.54

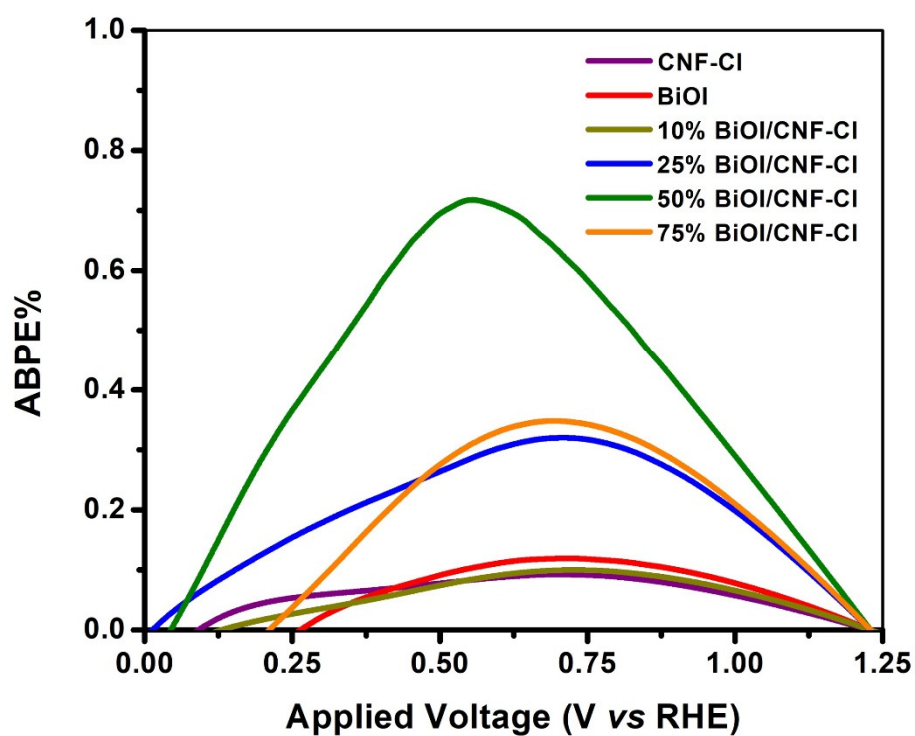


**Figure S5.** ABPE % vs RHE plot under AM1.5 G light irradiation ( $100 \text{ mW cm}^{-2}$ ) for pristine CNF-CI, pristine BiOI and BiOI/CNF-CI composites.

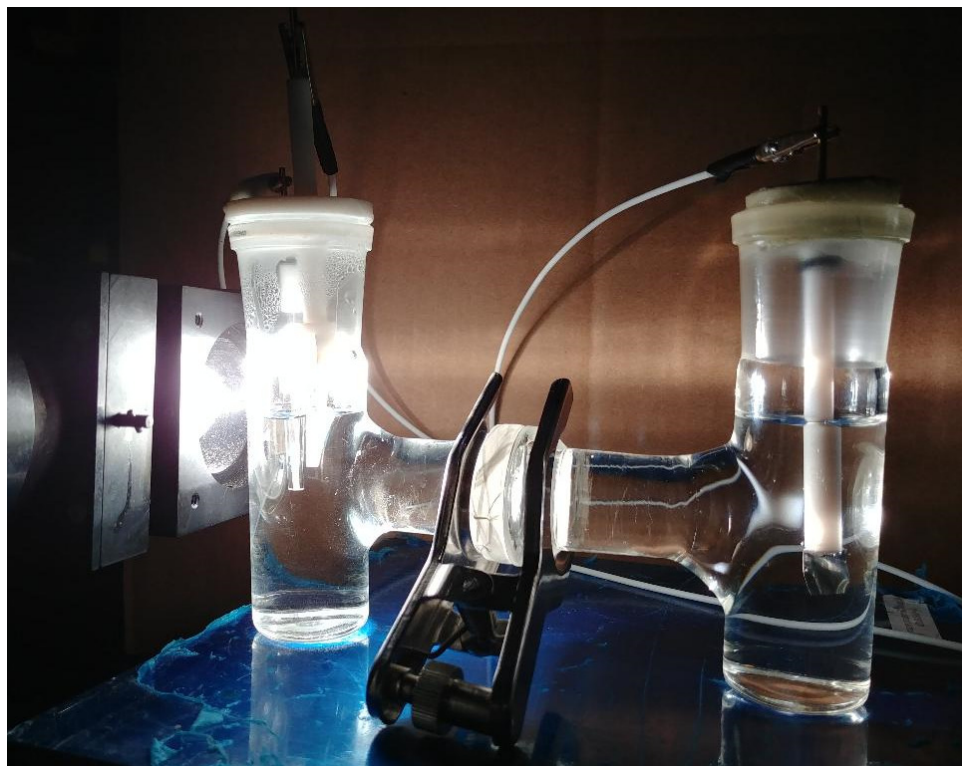


**Figure S6.** Photograph of photoelectrochemical water splitting cell (H-cell) irradiated under AM1.5 G irradiation.

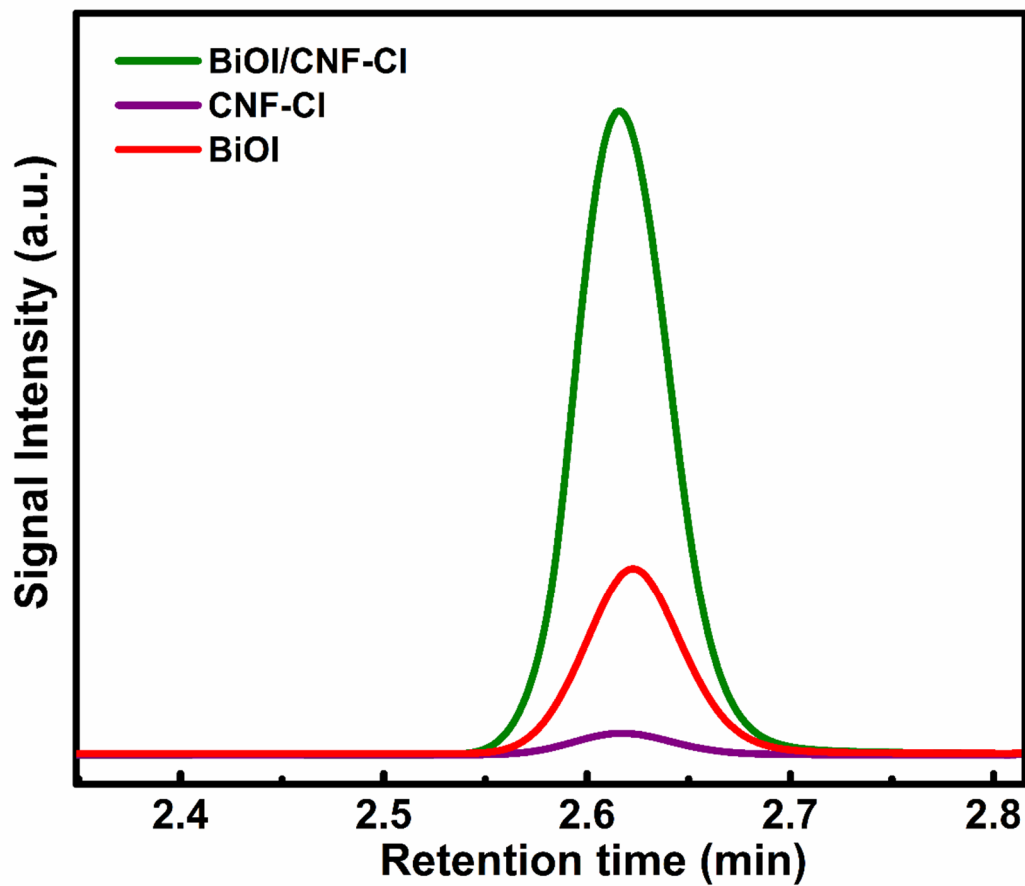


**Figure S7.** GC chromatogram of gaseous product collected at Pt counter electrode in photoelectrochemical water splitting experiment.

### ***5.0 Reusability test***

Resilience and reusability are prime requirements for the deployment and mass market commercialization of photocatalytic materials. To investigate the reusability of the developed BiOI/CNF-Cl heterostructure, the photocurrent response of previously used photoanodes was measured after each measurement. Prior to measurements, FTO deposited material was washed gently with water followed by drying at 85 °C. The photocurrent density of reused BiOI/CNF-Cl heterostructured material remains almost identical to freshly prepared BiOI/CNF-Cl, which demonstrate robustness and long-term reusability of material (Figure S10 in ESI†). Further, reused material was characterized with DRS, XRD to investigate any change in optical absorption profile and phase structure (Figures S8 and S9 in ESI†). The DRS and XRD spectra of reused BiOI/CNF-Cl catalysts were almost identical to that of fresh catalyst, which imply the chemical, optical and structural attributes of materials do not change much during photoelectrochemical measurement.

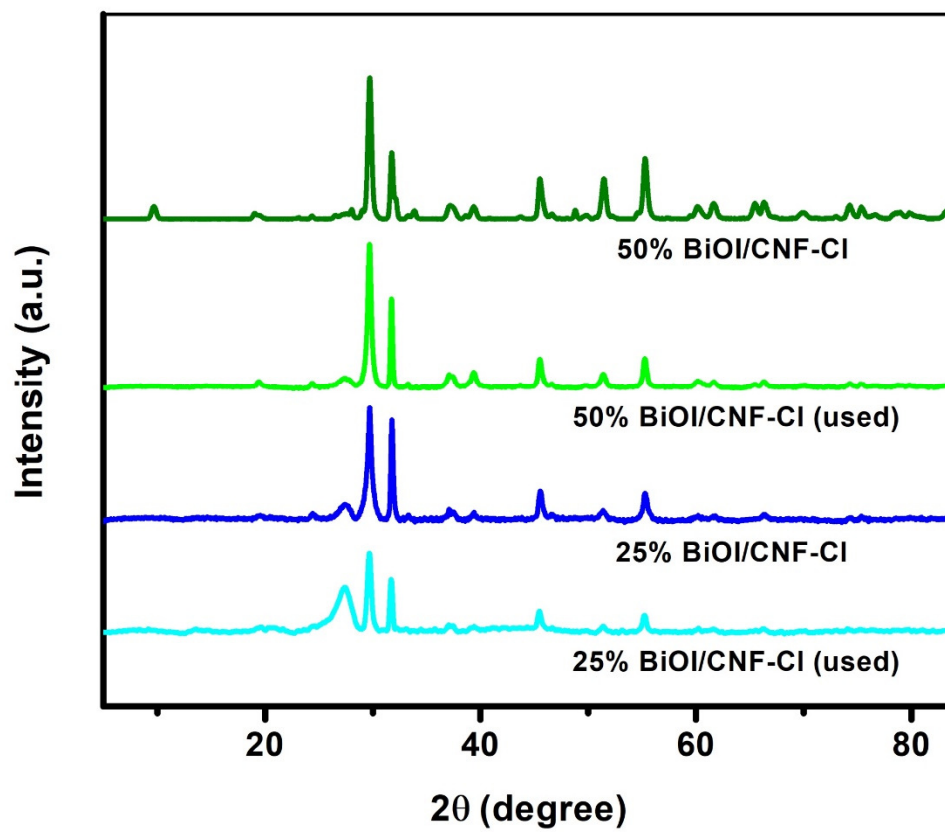


**Figure S8.** X-Ray diffractograms of BiOI/CNF-Cl heterostructures before and after several photoelectrochemical cycles.

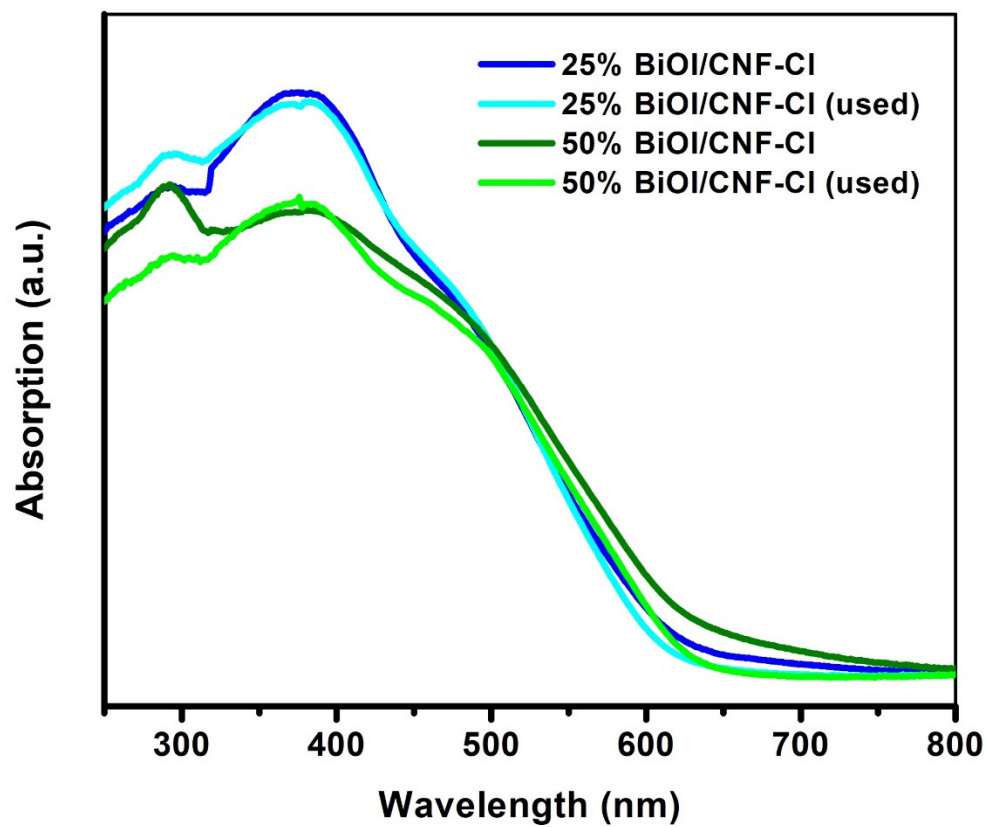


**Figure S9.** UV-Vis absorption spectra collected in diffuse reflectance (DR) mode for BiOI/CNF-Cl heterostructures before and after several photoelectrochemical cycles.

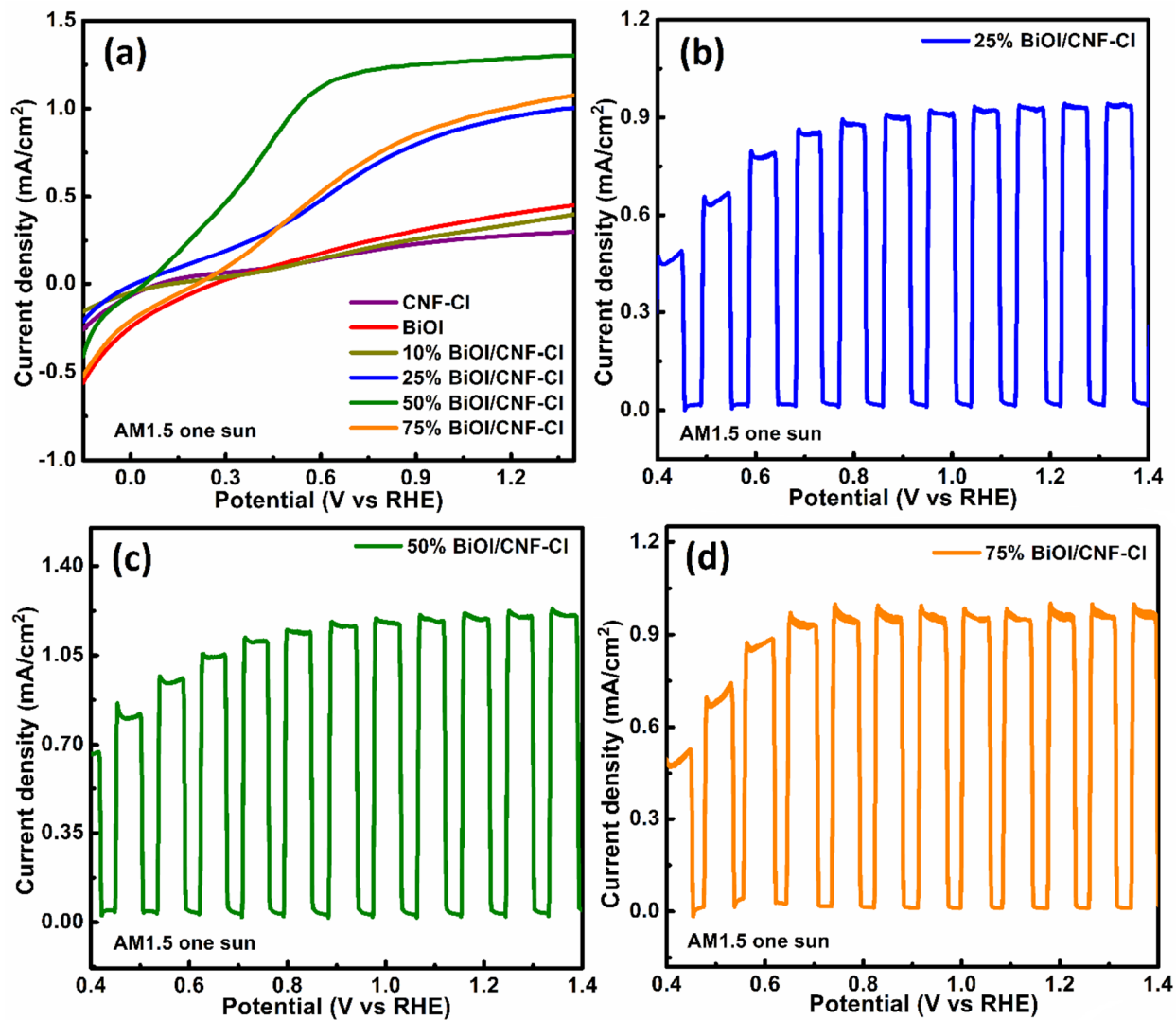


**Figure S10.** (a) Photocurrent of reused BiOI/CNF-Cl composite catalysts under AM1.5 G one sun illumination; (b), (c) and (d) Light on-off experiment for reused 25% BiOI/CNF-Cl, 50% BiOI/CNF-Cl and 75% BiOI/CNF-Cl photoanodes under AM1.5 G one sun illumination respectively.

#### References:

- [1] Y. Wang, Y. Di, M. Antonietti, H. Li, X. Chen, X. Wang, 2010 *Chem. Mater.* **22**, 5119-5121.
- [2] X. Lu, K. Xu, P. Chen, K. Jia, S. Liu, C. Wu, 2014 *J. Mater. Chem. A* **2**, 18924-18928.

- [3] C. Liu, Y. Zhang, F. Dong, A. Reshak, L. Ye, N. Pinna, C. Zeng, T. Zhang, H. Huang, 2017 *Appl. Catal. B* **203**, 465-474.
- [4] H. An, B. Lin, C. Xue, X. Yan, Y. Dai, J. Wei, G. Yang, 2018 *Chinese J. Catal.* **39**, 654-663.
- [5] S.-Y. Chou, C.-C. Chen, Y.-M. Dai, J.-H. Lin, W.W. Lee, 2016 *RSC Adv.* **6**, 33478-33491.
- [6] J. Di, J. Xia, S. Yin, H. Xu, L. Xu, Y. Xu, M. He, H. Li, 2014 *J. Mater. Chem. A* **2**, 5340-5351.
- [7] U.K. Thakur, A.M. Askar, R. Kisslinger, B.D. Wiltshire, P. Kar, K. Shankar, 2017 *Nanotechnology* **28**, 274001.
- [8] S. Yan, Z. Li, Z. Zou, 2009 *Langmuir* **25**, 10397-10401.
- [9] Y. Wang, R. Shi, J. Lin, Y. Zhu, 2011 *Energy Environ. Sci.* **4**, 2922-2929.
- [10] J. Zhang, M. Zhang, G. Zhang, X. Wang, 2012 *ACS Catal.* **2**, 940-948.
- [11] Y. Huang, H. Li, M.-S. Balogun, W. Liu, Y. Tong, X. Lu, H. Ji, 2014 *ACS Appl. Mater. Interfaces* **6**, 22920-22927.
- [12] O.K. Varghese, C.A. Grimes, 2008 *Sol. Energy Mater. Sol. Cells* **92**, 374-384.
- [13] Z. Chen, H.N. Dinh, E. Miller, 2013 *Photoelectrochemical water splitting*, Springer.
- [14] D.J. Inbaraj, B. Chandran, C. Mangalaraj, 2019 *Materials Research Express* **6**, 055501.
- [15] N.T. Hahn, S. Hoang, J.L. Self, C.B. Mullins, 2012 *ACS Nano* **6**, 7712-7722.